Article

New Insight into Geochemistry and Mineralogy of Deep Caves in Croatian Karst and Its Implications for Environmental Impacts

Dalibor Paar [1] , Stanislav Frančišković-Bilinski [2],[*] , Nenad Buzjak [3] and Krešimir Maldini [4]

1   Department of Physics, Faculty of Science, University of Zagreb, Bijenička cesta 32, 10000 Zagreb, Croatia;
     dpaar@phy.hr
2   Division for Marine and Environmental Research, Ruđer Bošković Institute, Bijenička cesta 54,
     10000 Zagreb, Croatia
3   Department of Geography, Faculty of Science, University of Zagreb, Trg Marka Marulića 19,
     10000 Zagreb, Croatia; nbuzjak@geog.pmf.hr
4   Main Water Laboratory (MWL), Department of Monitoring, Josip Juraj Strossmayer Water Institute,
     Ulica Grada Vukovara 220, 10000 Zagreb, Croatia; kresimir.maldini@institutjjs.hr
*   Correspondence: francis@irb.hr

Abstract: This study examines speleothems, sediments, rock, and water to assess geochemical and mineralogical processes in deep karst systems. Focusing on Slovačka jama cave (-1320 m deep) and the Velebita cave system (-1026 m deep), we identify elemental and mineralogical anomalies that provide valuable records of element transport, mineral formation, and paleoenvironmental changes. Heavy metal anomalies (Al, B, Co, Mn, Na, Tl, Ba, Be, Cr, Cu, Fe, K, Pb, Rb, Ti, U, Zn) at 300–400 m of depth in Slovačka jama indicate a complex interplay of geological conditions, geomorphological processes, atmospheric deposition, and potential anthropogenic influences. Factor analysis reveals two elemental associations: (1) Fe, Pb, Cu, and Zn, linked to terrigenous aluminosilicates, and (2) Cd, Cr, Mo, and Ni, suggesting airborne or geological sources. Mineralogical analysis confirms the dominance of calcite, with quartz, clay minerals, feldspars, magnetite, and goethite also detected. High magnetic susceptibility values in sediment-rich samples suggest Fe-rich mineral inputs from weathering, biogenic activity, or industrial sources. Ba anomalies in feldspar-rich samples and Sr accumulation at depth indicate distinct geochemical processes. These findings enhance our understanding of deep karst geochemistry, crucial for paleoenvironmental reconstructions and groundwater protection.

Keywords: Dinaric karst; deep caves; geochemistry; mineralogy; magnetic susceptibility

1. Introduction

The Croatian karst is primarily situated in the Dinaric karst, globally recognized as the locus typicus of Classical Karst, with a smaller portion extending into isolated karst areas of the Pannonian Basin [1]. Karst landscapes are among the most complex and hydrologically dynamic environments on Earth, characterized by high permeability, rapid water flow, and intricate interactions between surface and underground processes [2,3]. Despite its significance, the geochemistry and mineralogy of Croatian caves remained largely unexplored until recent years.

To address this research gap, a study was launched in 2016 with the aim of identifying speleothem proxies suitable for paleoenvironmental reconstructions [4]. The primary focus was to analyze the elemental composition and mineralogy of speleothems from various Croatian karst sites and assess how distinct climatic, geological, geomorphological, and hydrological conditions influence their characteristics. A total of 37 speleothem

samples from 32 caves across different geomorphological and climatic zones were analyzed. The elemental composition of 30 elements was determined using ICP-MS, while mineral phases—including calcite, quartz, dolomite, muscovite/illite, chlorite, and plagioclase—were identified via XRD. Among the most abundant elements, in addition to calcium, those exceeding 500 mg/kg included Al, Fe, Si, and Mg. Statistical analysis using boxplot methods revealed significant anomalies in the deep caves of Northern Velebit, particularly in Lukina jama, where extreme values were recorded for Pb, Cu, Zn, Mn, Ni, Cr, Co, Ba, K, Mg, Li, Be, Al, U, Si, Ti, W, Fe, and As. These findings align with previous studies indicating that deep karst environments often record significant geochemical anomalies due to their complex hydrological and tectonic histories [4,5].

Given that the most pronounced anomalies among 32 studied caves in different parts of Croatia were identified in our earlier study [4] in the deep caves of Velebit Mountain, a new study was initiated to investigate geochemical and mineralogical variations at depths of up to 1320 m in Slovačka jama cave and 1026 m in the Velebita cave system. These caves, which contain the highest anomalies of heavy metals and other chemical elements among all 32 studied caves from different parts of Croatia, are located within a geologically complex karst terrain shaped by intensive tectonics, particularly during the Neotectonic period, which, in conjunction with prolonged karstification, has resulted in intricate subsurface structures (Figure 1). Recent research suggests that such deep cave environments provide valuable records of past climatic and geochemical conditions, making them critical sites for paleoenvironmental studies [6,7]. Sample 107 from Slovačka jama cave, the most anomalous site, showed elemental anomalies consistent with those found in our previous research [4], where this cave was analyzed along with other Croatian caves. Since both caves are situated within the same geological units and are only about 2 km apart, their geochemical profiles—reflected in speleothems, rocks, and sediments—are expected to be highly similar. Therefore, paleodata obtained from one cave should be applicable to the other, justifying our approach of evaluating both caves together in this study.
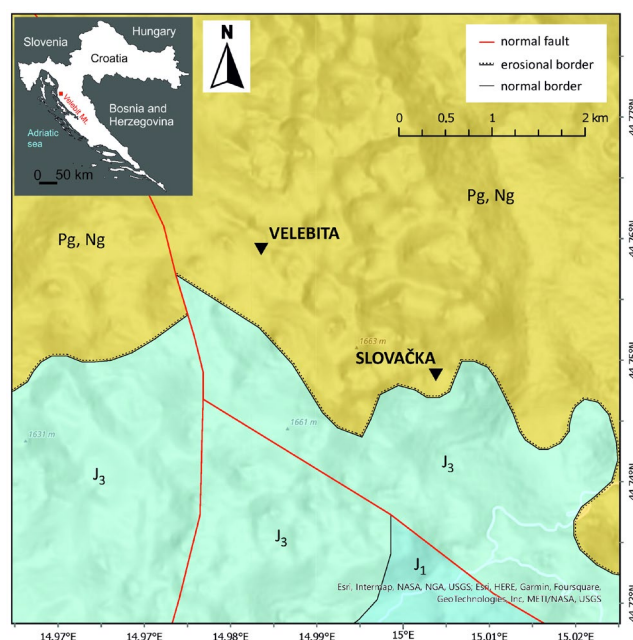

Figure 1. Position of Velebita cave system and Slovačka jama cave on the geological map of Velebit Mt. Lithostratigraphical legend: J_1—limestones and dolomites (Lower Jurassic), J_3—limestones and dolomites (Upper Jurassic), Pg, Ng—carbonate breccia (Paleogene, Neogene). Map: Croatian Geological Survey (2009): Geological map of the Republic of Croatia M 1:300,000, Zagreb.

The Velebita and Slovačka jama caves are located in the strictly protected Northern Velebit National Park and are difficult to access due to the absence of nearby roads. Velebita lies approximately 6 km from the village of Krasno, while Slovačka is about 8 km from Krasno and a similar distance from the nearest coastal settlement. Both caves are predominantly vertical (Figure 2), making them unsuitable for tourism and accessible only to skilled speleologists and researchers. Consequently, entry is rare, occurring only during occasional speleological expeditions, typically a few times per decade.
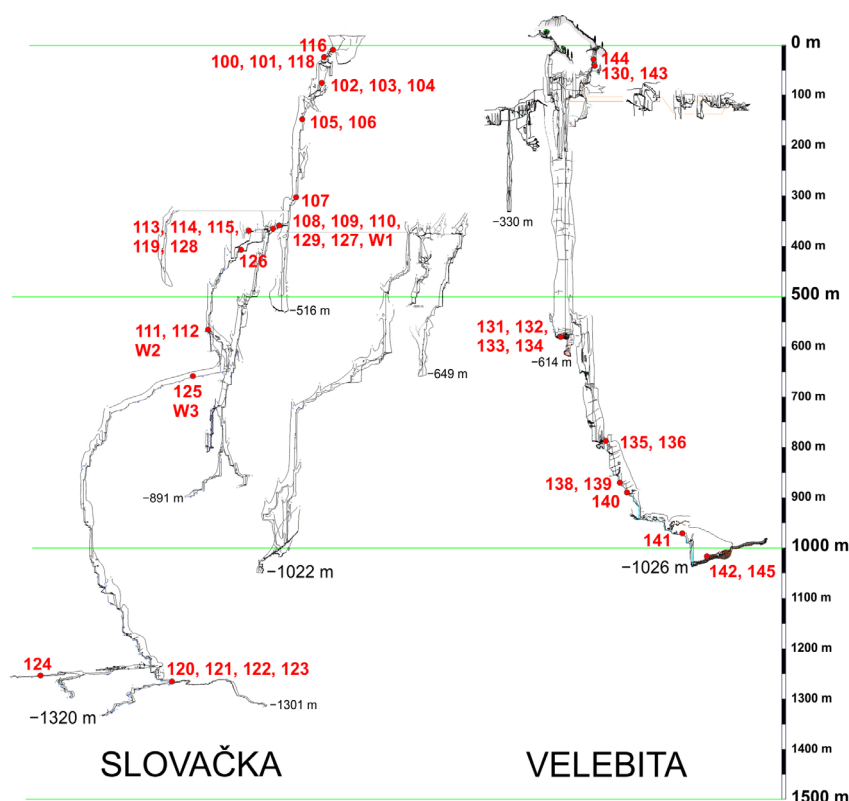
Figure 2. Sampling locations in Slovačka jama and Velebita cave system, Velebit Mt., Croatia. Red numbers refer to samples. Map: Speleological Committee of CMA (1995–2017).

The study of karst systems is not only important for understanding past environmental changes, but also has direct implications for water resource management. Karst aquifers are highly vulnerable to contamination due to their rapid recharge and direct connectivity between surface and groundwater systems [8]. It is estimated that approximately 25% of the world's population relies on groundwater extracted from karst aquifers [9]. Understanding the hydrogeochemical dynamics of these systems is particularly challenging due to their extreme heterogeneity [10,11]. Investigations in deep caves offer a unique opportunity for in situ sampling, measuring, and analyses of karst processes in deep karst (>1.000 m), shedding light on the mechanisms controlling element mobility, mineral formation, and potential anthropogenic impacts [12] influencing epiphreatic and phreatic zones important for regional aquifer characteristics.

In our study, we expand upon previous research by analyzing multiple sampling media—including speleothems, cave clastic sediments, and water chemistry—to assess their geochemical and mineralogical properties and identify potential interactions. Such multi-proxy approaches remain relatively rare in karst research, particularly concerning cave sediments and water chemistry. However, several relevant studies provide useful comparisons. For instance, Rozkowski et al. [13] examined the migration and concentration of heavy metals in infiltration waters within a carbonate massif, linking these variations to

both natural mobility and anthropogenic influences. Similarly, Pons-Branchu et al. [14] utilized urban speleothems to reconstruct heavy metal pollution histories in shallow groundwater systems, demonstrating how speleothem chemistry can serve as a long-term record of environmental changes. Other studies have explored the role of cave sediments and particulate matter in element transport, with Allan et al. [15] analyzing lead concentrations and isotopic compositions in Belgian caves to distinguish between anthropogenic and natural sources. More recently, Xu and Zeng [16,17] investigated heavy metal contamination in cave water and suspended particulate matter, respectively, underscoring the importance of geochemical monitoring in karst systems.

The primary aim of this study is to systematically investigate geochemical and mineralogical variations in deep karst cave environments, assess the potential interactions between different sampling media, and evaluate their implications for paleoenvironmental reconstructions and pollution monitoring.

2. Materials and Methods

2.1. Sample Preparation and Analysis

The speleothems for this study were collected with minimal disturbance to the cave environment, ensuring that natural formations remained intact. The sampling locations in the Velebita cave system and Slovačka jama cave are shown in Figure 2 and Table 1. Samples were collected from sites where carbonate precipitation and karst drainage networks facilitate speleothem growth [18–21]. These locations were carefully selected to ensure representative data on geochemical and mineralogical processes within the deep karst environment.

Table 1. List of samples, types, and locations in Slovačka jama cave (S) and Velebita cave system (V).

Cave	Depth (m)	Speleothem	Sediment	Rock	Water
S	0		116		
S	10		100	101, 118	
S	65		102, 104	103	
S	140		105	106	
S	285		107		
S	350	108, 119, 129	110, 127	109	
S	360	114	128	113, 115	W1
S	405		126		
S	550		112	111	W2
S	620	125			W3
S	1250		124		
S	1254	120, 121		122, 123	
V	30	144A		144B	
V	50	143	130		
V	580	131	133, 134	132	
V	786		135, 136		
V	860	138, 139			
V	880			140	
V	975			141	
V	1000	142, 145			

Samples were carefully handled to prevent contamination, washed with distilled water, air-dried, and then homogenized using a Retsch RM 200 mortar grinder (Retsch, Haan, Germany). Whole speleothems were crushed to obtain representative powders incorporating all growth layers. From these, 1 g of material was used for ICP-MS and XRD analysis.

For the elemental analysis of solid samples, 0.1 g of powdered sample was digested in a mixture of suprapur nitric and puriss hydrochloric acid, and heated in an Anton Paar Multiwave 3000 Oven (Anton Paar, Graz, Austria) following ISO 11466 standards. ICP-MS (Elan 9000, Perkin Elmer, Shelton, CT, USA) was used to determine elemental concentrations, employing internal standards (Ge, Rh, In, Re) according to ISO 17294-1 and ISO 17294-2. Precision (RSD) was within 10%, and accuracy was verified using reference material (RTC CNS392-050), with results aligning within 15% of certified values. Only two samples (64, 70) had values below the quantification limit for Tl (5.4%).

Mineralogical composition was identified using X-ray diffraction (XRD) with a Philips PW3040/60 X'Pert PRO diffractometer (Philips Analytical, Almelo, The Netherlands) and analyzed via Powder Diffraction File (1997) and X'Pert HighScore software (version 5.2). Semi-quantitative mineralogy followed [22].

Magnetic susceptibility (MS) was measured using an SM30 (ZH Instruments, Brno, Czech Republic) susceptibility meter, capable of detecting low-magnetic and diamagnetic materials such as limestone and quartz. Measurements were performed three times per sample, with the mean value recorded to ensure accuracy.

Electroconductivity and pH were measured using a SevenMulti instrument (Mettler Toledo, Schwerzenbach, Switzerland) in accordance with standards HRN EN ISO 10523:2012 and HRN EN 27888:2008. Turbidity was analyzed with a 2100 N turbidimeter (Hach, Loveland, CO, USA) following the standard method SM:1995-2130 B.

Anions and cations were quantified via ion chromatography using an ICS 3000 system (Dionex, Sunnyvale, CA, USA) according to standards HRN EN ISO 10304-1:2009 and HRN EN ISO 14911:2001. Alkalinity was determined using a Mantech PC-Titrate system (Guelph, ON, Canada) following standard HRN EN ISO 9963-1:1998. Total dissolved solids and HCO_{3-} concentrations were calculated as per [23,24].

Orthophosphates were analyzed with a Lambda 25 spectrophotometer (PerkinElmer, Shelton, CT, USA) in accordance with standard HRN EN ISO 6878:2008. Total organic carbon (TOC) and total nitrogen (TN) were measured using a TOC-VCPH analyzer with a TNM-1 unit (Shimadzu Corporation, Kyoto, Japan) following standards HRN EN 1484:2002 and HRN EN 12260:2008. Chemical oxygen demand (COD) was determined using the titrimetric method in compliance with standard HRN EN 8467:2001.

Total phosphorus (TP) was measured via inductively coupled plasma mass spectrometry (ICP-MS, Elan 9000, PerkinElmer, USA), utilizing a 20 $\mu g \, L^{-1}$ In solution as an internal standard, according to HRN ISO 17294-2:2003.

To define hydrochemical facies, a Piper diagram was used (generated with USGS software GW Chart, version 1.24.0.0), which illustrates the relationships among major anions and cations (Ca^{2+}, Mg^{2+}, Na^+, K^+, HCO_{3-}, CO_3^{2-}, SO_4^{2-}, and Cl^-).

2.2. Statistical Analysis

Statistical analyses were conducted using Statistica 6.0 [25] and included the following:

(a) Descriptive Statistics: Basic parameters (mean, median, standard deviation, skewness, kurtosis) were calculated to summarize the dataset. Pearson's correlation coefficients were determined to assess relationships between elements ($p < 0.05$).

(b) Boxplot Analysis: Used to identify anomalies in sediment samples based on interquartile range, with outliers and extreme values defined according to Tukey [26] and Reimann et al. [27].

(c) Cluster Analysis (Q-mode): Performed to group similar samples using a hierarchical method, distinguishing sample clusters rather than elemental correlations [28].

(d) Factor Analysis: Applied to reduce variable complexity and identify key natural or anthropogenic influences, assuming correlations between multiple elements are driven by a smaller set of main factors [29,30].

3. Results

3.1. Mineralogical Analysis Using X-Ray Diffraction

Mineralogical analysis using X-ray diffraction (XRD) identified 10 minerals across the samples: carbonates (calcite, dolomite), silicates (quartz, clay minerals—kaolinite, muscovite, chlorite, montmorillonite, and feldspar—plagioclase), spinels (magnetite), and oxihydroxides (goethite). This method is qualitative, with a detection limit of ~5%.

As expected, calcite was present in all samples due to the karstic environment, where speleothems form through limestone dissolution and carbonate precipitation (Table A1). Dolomite appeared in only three rock samples from Slovačka jama (samples 118, 122, 123), suggesting localized geochemical variations. In eight samples, only calcite was detected (e.g., 101, 111, 113).

Quartz, the second most abundant mineral, was found in 36 of 45 samples, likely originating from fine-grained clastic sediments introduced into the cave system [4]. Similar findings were reported in karstic river sediments [31].

Among clay minerals, muscovite and chlorite were most common, followed by kaolinite and montmorillonite. Samples containing at least two clay minerals (e.g., 105, 107, 110) often coincided with geochemical anomalies and high magnetic susceptibility (MS). Notably, samples 105 and 107, from the same vertical channel of Slovačka jama, displayed strong similarities despite a 145 m elevation difference. The abundance of clay minerals suggests a potential paragenetic relationship between quartz and kaolinite. This observation is consistent with the findings of Chen et al. [32], who proposed that quartz cementation likely resulted from feldspar dissolution, the illitization of smectite and kaolinite, and the pressure solution of quartz grains.

Feldspars (plagioclase) were detected in only four samples (112, 126, 130, 133), all from channel-bottom sediments in Slovačka jama and the Velebita cave system. Among Fe-bearing minerals, magnetite and goethite were identified in samples from Slovačka jama, with sample 110 being the only one containing both. These minerals may indicate past hydrothermal influences or iron mobilization within the cave system.

The relationships between mineralogical composition, ICP-MS element concentrations, and magnetic susceptibility will be further explored in the discussion.

3.2. ICP-MS Analysis, Magnetic Susceptibility, and Elemental Anomalies

The ICP-MS analysis results for speleothems and water samples are presented in Tables A2 and A3. While elemental concentrations in speleothems will be statistically analyzed in later sections, water sample data were not statistically evaluated due to the limited number of results (n = 3).

The results of physico-chemical parameters, nutrients, ions, total nitrogen (TN), total phosphorus (TP), chemical oxygen demand (COD), and total organic carbon (TOC) in the three water samples are presented in Table A4.

Magnetic susceptibility (MS) values, expressed in 10^{-3} SI units, range from 0.000 to 0.168, with the highest value recorded in sample 107 (Table A5). MS variations will be discussed in relation to elemental composition in later sections.

Elemental anomalies identified using the boxplot statistical method (Figure 3) indicate that sample 107 has the highest number of anomalies, followed by 127.
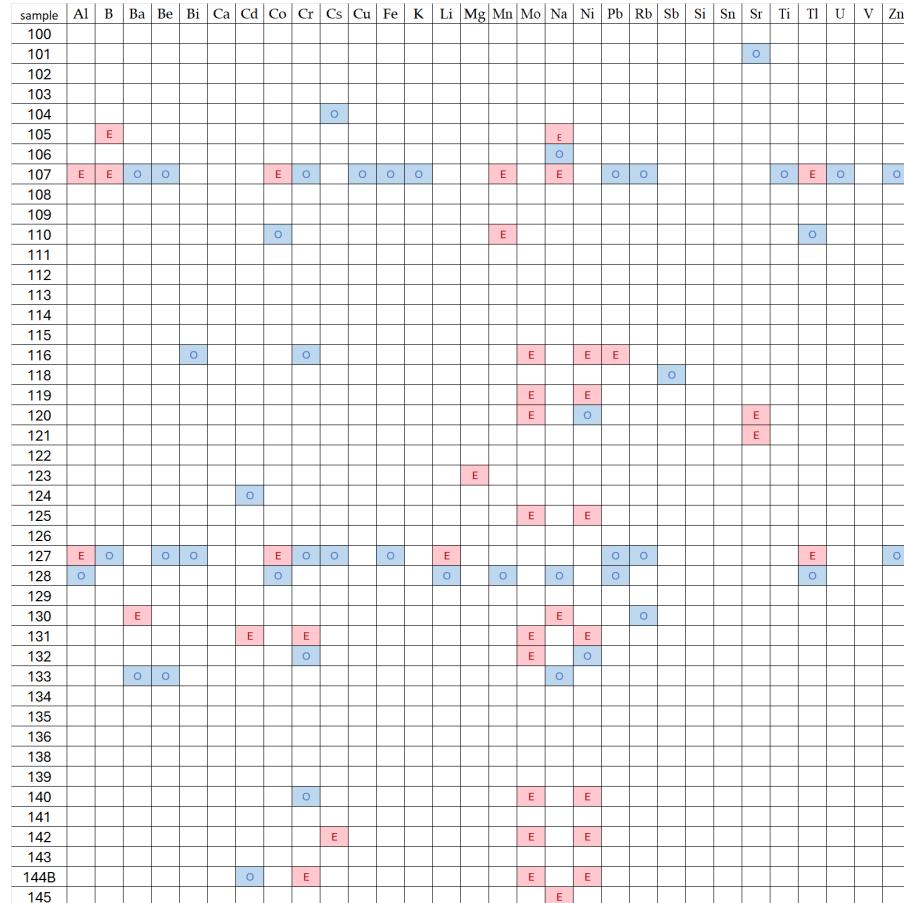
sample	Al	B	Ba	Be	Bi	Ca	Cd	Co	Cr	Cs	Cu	Fe	K	Li	Mg	Mn	Mo	Na	Ni	Pb	Rb	Sb	Si	Sn	Sr	Ti	Tl	U	V	Zn
100																														
101																										O				
102																														
103																														
104										O																				
105		E																E												
106																		O												
107	E	E	O	O			E	O			O	O	O			E		E		O	O				O		E	O		O
108																														
109																														
110								O								E												O		
111																														
112																														
113																														
114																														
115																														
116				O				O								E			E	E										
118																						O								
119																E			E											
120																E			O											
121																								E						
122																														
123														E																
124					O																									
125																E			E											
126																														
127	E	O		O	O		E	O	O		O		E							O	O			E			E			O
128	O							O				O			O			O		O				O			O			
129																														
130		E																E			O									
131					E		E											E		E										
132								O										E		O										
133			O	O															O											
134																														
135																														
136																														
138																														
139																														
140								O										E		E										
141																														
142										E								E		E										
143																														
144B					O		E											E		E										
145																		E												

Figure 3. Anomalies determined by boxplot method (E: extremes—presented in red color, O: outliers—presented in blue color).

Outliers and extremes were observed for multiple elements, suggesting localized geochemical or environmental influences. These patterns will be further explored in the discussion.

3.3. Q-Modality Cluster Analysis

The Q-mode cluster analysis results are presented in Tables A6 and A7. Three clusters were identified:

- Cluster 1 (deepest, avg. depth 664.25 m): Composed of eight sediments, four speleothems, and four rock samples, showing a moderate concentration of heavy metals.
- Cluster 2 (intermediate, avg. depth 440.25 m): Contains 10 rocks, nine speleothems, and one sediment sample, with the lowest heavy metal concentrations.
- Cluster 3 (shallowest, avg. depth 323.89 m): Includes eight sediments and one rock sample, exhibiting the highest heavy metal concentrations (except for Ni), suggesting accumulation near the surface due to airborne pollution, soil leaching, and surface runoff.

Both caves are formed within massive Velebit limestone breccias (previously referred to as Jelar deposits) down to a depth of approximately 250 m, where they transition

gradually into intensely fractured to layered Upper Jurassic dolomitic limestones [33]. Between depths of 400 and 980 m, limestone breccias once again dominate, but they occur in irregular alternations with layered limestones of a normal stratigraphic sequence. The presence of breccias at depths of up to 980 m below the surface is explained by a model of tectonized zones filled with Velebit breccias, which intersect Jurassic limestones in a normal sequence.

Comparing the available literature data with the average depth of our clusters reveals that the shallowest, Cluster 3, is located within fractured to layered Upper Jurassic dolomitic limestones. The intermediate Cluster 2 and the deepest Cluster 1 are positioned within limestone breccias that alternate irregularly with layered limestones. Thus, the cave's rock composition is unlikely to have a significant influence on heavy metal concentrations, while the other processes mentioned are more likely to play a dominant role.

Heavy metals appear to migrate downward, accumulating first in shallow cave sections before being rinsed and redeposited in deeper zones. These transport mechanisms require further investigation.

Strontium concentrations notably increase in the deepest sections, but current data are insufficient to draw firm conclusions, warranting further research. Additionally, calcium concentrations in speleothems are lowest in shallow sections, nearly four times lower than in the middle depth, where they peak.

3.4. Factor Analysis

Factor analysis was performed on 16 variables, including sample depth and elemental concentrations (Al, Be, Ca, Cd, Co, Cr, Cu, Fe, Li, Mn, Ni, Pb, Si, Sr, Zn). The results explained 83.7% of the total variability, indicating a strong statistical model. Factor scores (Table A9) indicate the degree of influence of each factor on individual samples, while factor loadings (Table A8) reveal relationships between variables.

Interpretation of Factors

Factor 1: Dominated by the aluminosilicate component, indicating high influence from soil and non-carbonate rocks. Ca shows a strong negative correlation, while Fe and Mn likely originate from natural aluminosilicates. Zn, Pb, and Co may have either natural or anthropogenic sources, but strongly correlate with this factor.

Factor 2: Primarily associated with Cd, Cr, and Ni, forming a distinct elemental group. Their origin could be either atmospheric deposition from distant pollution sources or natural geological processes, differing from elements in Factor 1.

Factor 3: Shows negative correlations with depth and Sr, consistent with Q-mode cluster analysis, which indicates that Sr concentrations increase with depth.

These factors offer valuable insights into the geochemical processes influencing element distribution within the studied cave system. However, a more detailed characterization of mineral associations related to specific factors is not possible due to the limitations of the available XRD method, which has a detection limit of >3–5%.

4. Discussion

This section integrates mineralogical, geochemical, and geophysical data to explain the origin of detected elements and minerals, their distribution, and interactions within the cave system.

4.1. Mineralogy and Magnetic Susceptibility (MS) Relationships

Samples containing only calcite (or calcite + dolomite) exhibited very low MS values ($\leq 0.002 \times 10^{-3}$ SI units) and showed few or no elemental anomalies. A notable exception was sample 123, where an Mg anomaly coincided with the presence of dolomite, confirming

its natural origin. This sample, collected from a horizontal channel at the bottom of Slovačka jama, suggests the presence of dolomitic bedrock at depth, though current geological maps lack subsurface detail.

In contrast, samples containing clay minerals displayed higher MS values and numerous elemental anomalies. The most abundant clay minerals were chlorite and muscovite, with kaolinite and montmorillonite present in smaller amounts. Chlorite, commonly found in metamorphic and volcanic environments, is known to contain Fe and Mn, which may explain the observed high MS values. It is likely formed through low-grade metamorphism or the weathering of mafic minerals (e.g., pyroxenes, amphiboles, biotite).

4.2. Elements and Magnetic Susceptibility (MS) Relationships

Table A10 presents the correlations between magnetic susceptibility (MS) and chemical elements in the studied samples. MS exhibits strong to excellent correlations with Al, Ba, Be, Bi, Ca, Co, Cu, Fe, Li, Mn, Pb, Rb, Ti, Tl, and Zn, suggesting that MS can serve as a reliable proxy for detecting locations with elevated concentrations of these elements. The use of MS in environmental research as a promising, fast, and cost-effective method for detecting heavy metal anomalies is relatively new. It was only recently applied for the first time in Croatia [34]. Therefore, the correlations between MS and elemental concentrations in this study represent a significant step toward the routine application of this method in karst research.

4.3. Potential Sources of Clay Minerals and Heavy Metals

The clay minerals in the samples studied may originate from multiple sources:

1. Terra rossa contribution: Similar to findings from Istria [35], terra rossa in karst regions often forms from insoluble residues of limestone and dolomite, but can also contain aeolian dust, volcanic debris, and transported sedimentary particles. These external sources may have introduced heavy metals over geological timescales.
2. Aeolian and volcanic inputs: Past atmospheric processes could have deposited metal-rich dust and volcanic ash, leading to localized heavy metal anomalies.
3. Hydrothermal activity: Though not confirmed, hydrothermal processes might have contributed to mineral transformations and heavy metal enrichment in deeper cave sediments.

4.4. Feldspars and Their Geochemical Significance

Feldspars (plagioclase) were detected in only four samples, often alongside clay minerals. While no major anomalies were associated with feldspar-rich samples, Ba anomalies were identified in samples 130 and 133. Since alkaline barium feldspars can form through Ba substitution for K in feldspar structures, it might be possible that crystallization processes in igneous or metamorphic rocks played a role in Ba enrichment, but to confirm this, additional research is needed. With the available XRD method, it is not possible to characterize minor minerals present in amounts below 3–5%. Therefore, it remains uncertain whether Ba originates from barite or is present in adsorbed forms.

4.5. Iron Minerals and Their Origins

Two Fe-rich minerals were detected:

1. Magnetite (spinels)—Found in cave sediments, with the following possible origins:
   (a) Natural sources, such as weathering of bauxites (known to occur in Velebit Mt.).
   (b) Biogenic activity, as some microorganisms can precipitate magnetite.
   (c) Anthropogenic pollution, transported via airborne deposition.

2. Goethite (oxyhydroxides)—Typically forms through lateritic weathering and was found in samples where Fe anomalies were detected.

Samples 107 and 127, both from Slovačka jama, exhibited Fe anomalies and contained magnetite, suggesting an unusual geochemical environment in these sediments.

4.6. An Unusual Geochemical Outlier

Sample 107 (285 m depth, Slovačka jama) displayed the following:

- The highest MS value (0.168×10^{-3} SI units).
- A complex mineralogical composition (calcite, quartz, all four clay minerals, magnetite).
- Multiple elemental anomalies, including extremes for Al, B, Co, Mn, Na, Tl and outliers for Ba, Be, Cr, Cu, Fe, K, Pb, Rb, Ti, U, Zn.

These anomalies suggest a unique depositional or geochemical process, potentially involving multiple metal sources (natural and anthropogenic), deep sediment accumulation, and prolonged geochemical transformations. Further geochemical and isotopic studies are needed to fully understand its formation.

4.7. Factor Analysis and Elemental Associations

Factor analysis revealed a distinct grouping of Cd, Cr, and Ni, separate from other heavy metals. This suggests the following:

- Different sources or transport mechanisms compared to Zn, Pb, and Co.
- Possible atmospheric deposition (long-range transport of industrial pollutants).
- Alternatively, a unique natural geological source distinct from the aluminosilicate fraction.

Our results indicate that heavy metal anomalies in cave sediments and speleothems can be attributed to a combination of natural geochemical processes and potential atmospheric deposition. Similar findings were reported by Rozkowski et al. [13], who examined heavy metal transport within the unsaturated and saturated zones of a carbonate massif in Poland. Their study highlighted the influence of infiltration processes on metal migration, which aligns with our observations of metal transport from shallow to deep cave sections in Slovačka jama and the Velebita cave system. The accumulation of elements like Pb, Zn, and Cu in cave sediments suggests both allochthonous input (surface-derived material) and internal redistribution within the karst system.

Moreover, our analysis supports the idea that speleothems can serve as long-term environmental archives, recording changes in metal concentrations over time. Pons-Branchu et al. [36] demonstrated that speleothems in urban settings provide valuable records of historical heavy metal pollution, showing enrichment in Pb, Mn, V, Cu, Cd, and Al due to anthropogenic contamination. While our study is focused on deep karst environments rather than urban speleothems, the detection of Cd, Cr, and Ni as a distinct elemental association (factor analysis) raises the possibility of airborne metal deposition from distant pollution sources, a hypothesis also considered in their research.

While Pb anomalies in our samples could originate from natural sources (aluminosilicate components), the presence of additional metals associated with industrial activity suggests that long-range atmospheric transport may also contribute. The role of lead in karst environments has been extensively studied, with Allan et al. [15] demonstrating how Pb concentrations and isotopic ratios in speleothems can be used to trace atmospheric pollution since the Industrial revolution. Further isotopic analysis could help differentiate between these sources.

4.8. Geochemical Characterization of Three Water Samples

Dissolved anions and cations in water samples from Slovačka jama cave indicate that the groundwater belongs to the calcium–bicarbonate type (Ca–HCO$_3$) (Figure 4). Since the water samples have nearly identical compositions in terms of anions and cations, all three points are closely aligned in almost the same position on the Piper diagram. The measurement results for physico-chemical parameters, nutrients, ions, total organic carbon (TOC), and chemical oxygen demand (COD) at the three sampling sites are presented in Table A4. Since water in karst areas is buffered by carbonate, all three analyzed water samples are of a slightly alkaline type, with pH values ranging between 7.7 and 7.9. The dominant cation in all three water samples is Ca, with low concentrations of Mg, Na, and K. Low concentrations of ammonium, nitrates, nitrites, orthophosphates, TN, TP, and TOC indicate that the water in the Slovačka jama cave is not significantly impacted by pollution.

Figure 4. Piper diagram of three water samples from Slovačka jama cave. Data for construction of Piper diagram are taken from Table A3 (ICP-MS and ion chromatography results of water samples) for Ca^{2+}, Mg^{2+}, Na$^+$, and K$^+$, while data for all other ions are taken from Table A4, which presents results of physico-chemical parameters, nutrients, ions, TN, TP, COD, and TOC.

The solubility and transport of elements from speleothems are influenced by pH values and redox conditions. The relatively low concentrations of elements in the water samples suggest oxidative conditions, favoring their deposition in speleothems. This deposition is further supported by the relatively low concentrations of total organic carbon (TOC).

The mean values of pH, nitrates, total nitrogen, and all measured elements—except for Ba and Sr—were higher than the average values reported for Biokovo Mt. springs by [37]. This difference can be attributed to variations in geological composition, as the Velebit region contains both carbonate and non-carbonate rocks, such as clastic formations. Importantly, all measured indicators in the three water samples remained below the maximum permitted values.

Overall, the combined use of mineralogical, geochemical, and statistical methods provided a comprehensive understanding of element distribution in deep karst environments, highlighting both natural and anthropogenic influences on cave sediments.

5. Conclusions and Future Research

This study highlights the complex geochemical interactions in deep karst environments, with speleothems and sediments serving as important archives of elemental transport and potential pollution pathways. Our results align with findings by Rozkowski et al. [13], Pons-Branchu et al. [36], and Allan et al. [15], all of whom investigated metal migration and accumulation in carbonate environments. The detection of heavy metal anomalies in sediments and speleothems suggests that karst systems are influenced by both natural geochemical processes and possible anthropogenic inputs.

Mineralogical analysis confirmed that calcite is the dominant mineral in all samples, as expected in a karst environment, while quartz was present in most samples, likely introduced via fine-grained clastic sediments. Clay minerals, including muscovite, chlorite, kaolinite, and montmorillonite, were found to be associated with higher magnetic susceptibility (MS) and heavy metal anomalies, indicating their role in metal transport. The presence of iron minerals such as magnetite and goethite, particularly in cave sediments, points to multiple possible origins, including natural sources such as bauxites, biogenic activity, or even airborne pollution.

Geochemical and statistical analyses provided additional insights into element distribution and transport within the cave system. Samples composed solely of calcite or calcite with dolomite exhibited the lowest MS values, indicating minimal influence from non-carbonate materials, whereas samples containing clay minerals displayed elevated MS values and a high number of elemental anomalies, supporting the hypothesis that clays play a significant role in metal retention. Boxplot analysis identified the highest number of anomalies in samples 107 and 127, suggesting a complex geochemical environment. Q-mode cluster analysis revealed that heavy metals are more concentrated in shallow cave sections, likely due to airborne deposition or surface leaching, with subsequent transport and accumulation in deeper parts of the cave system. Factor analysis identified cadmium, chromium, and nickel as a distinct group, indicating a different origin from other heavy metals, potentially related to atmospheric deposition or specific geological sources.

This research has advanced the understanding of deep cave geochemistry, particularly since such data are lacking in both the Dinaric karst and karst worldwide. Given the Dinaric karst's significance, the studied region provides key insights into karst processes and supports remarkable geological and biological diversity. However, several aspects still require further investigation.

Future research should focus on the stable isotope analysis of heavy metals, particularly Pb, to better identify the sources of these anomalies. A detailed examination of element transport to and within the caves, including more detailed geological mapping at depth and seismic profiling, is essential. Additionally, continued monitoring of atmospheric deposition and the identification of distant pollution sources could provide insights into the long-range transport of pollutants. Expanding both the spatial and depth range of sampling will improve our understanding of metal transport mechanisms and their implications for karst hydrology and groundwater protection in anthropogenically impacted areas. Investigating the role of aeolian dust and past volcanic activity in mineral deposition would also help to better understand the origins of clay minerals and associated elements. However, since the study sites are located within the Northern Velebit National Park and a strict nature reserve, with no nearby human settlements or roads, the designation of new protection zones is unnecessary.

Appendix A

Table A1. Mineral (phase) composition of speleothem samples. Sign "+" means that sample contains this mineral.

Sample	Calcite	Quartz	Kaolinite	Muscovite	Chlorite	Montmorill.	Magnetite	Goethite	Plagioclase	Dolomite
100	+	+								
101	+									
102	+	+								
103	+	+								
104	+	+	+							
105	+	+		+	+	+				
106	+	+								
107	+	+	+	+	+	+	+			
108	+	+								
109	+	+								
110	+	+		+	+	+	+	+		
111	+									
112	+	+		+	+	+			+	
113	+									
114	+	+		+			+			
115	+	+	+	+			+			
116	+	+		+	+					
118	+	+								+
119	+	+	+	+		+				
120	+	+								
121	+	+		+	+					
122	+	+					+			+
123	+									+
124	+	+		+	+					

Table A1. *Cont.*

Sample	Calcite	Quartz	Kaolinite	Muscovite	Chlorite	Montmorill.	Magnetite	Goethite	Plagioclase	Dolomite
125	+	+								
126	+	+			+				+	
127	+	+	+		+		+			
128	+	+	+	+	+		+			
129	+	+								
130	+	+		+	+	+			+	
131	+	+								
132	+									
133	+	+		+	+				+	
134	+	+		+	+					
135	+	+	+							
136	+	+								
138	+	+								
139	+	+								
140	+									
141	+									
142	+	+								
143	+	+								
144A	+									
144B	+	+								
145	+									

Table A2. Results of ICP-MS analysis of 30 chemical elements in solid samples.

Sample	Al mg/kg	B mg/kg	Ba mg/kg	Be mg/kg	Bi mg/kg	Ca mg/kg	Cd mg/kg	Co mg/kg	Cr mg/kg	Cs mg/kg	Cu mg/kg	Fe mg/kg	K mg/kg	Li mg/kg	Mg mg/kg
100	473	0.679	6.95	0.033	0.236	81,855	0.054	0.391	3.78	0.436	1.62	1618	129	2.66	101
101	251	0.596	3.20	0.015	0.071	92,465	0.040	0.287	4.93	0.532	0.660	558	94.2	5.18	156
102	472	0.760	8.21	0.036	0.213	74,620	0.047	0.470	2.95	0.553	1.20	1387	136	2.75	200
103	375	0.253	3.60	0.020	0.098	86,836	0.044	0.350	3.52	1.0	0.831	793	56.8	2.72	92.6
104	3502	2.19	35.3	0.156	1.36	49,249	0.076	1.29	10.9	6.79	5.76	9876	731	14.1	377
105	4113	9.96	61.5	0.175	0.664	90,203	0.153	1.98	12.4	2.07	4.20	5570	1143	5.56	507
106	409	1.73	4.85	0.015	0.103	128,213	0.043	0.587	3.80	0.252	0.590	517	269	3.77	300
107	13,737	13.1	112	0.452	2.0	3732	0.374	5.64	31.9	4.56	9.30	26,293	1923	22.2	738
108	320	0.363	5.63	0.012	0.053	114,421	0.031	0.531	3.58	0.170	0.545	500	76.7	0.618	45.2
109	180	0.145	7.82	0.016	0.072	87,355	0.086	0.450	2.68	0.140	0.750	664	27.5	0.844	105
110	6171	4.90	71.2	0.273	1.12	26,950	0.443	3.44	20.2.	3.32	4.62	16,480	853	23.9	321
111	30.8	0.145	0.845	<0.005	0.023	106,600	0.017	0.293	2.34	<0.030	0.373	65.6	12.8	0.085	520

Table A2. *Cont.*

Sample	Al mg/kg	B mg/kg	Ba mg/kg	Be mg/kg	Bi mg/kg	Ca mg/kg	Cd mg/kg	Co mg/kg	Cr mg/kg	Cs mg/kg	Cu mg/kg	Fe mg/kg	K mg/kg	Li mg/kg	Mg mg/kg
112	1719	0.694	46.4	0.091	0.481	64,409	0.069	1.09	6.55	1.12	2.15	4898	569	3.06	389
113	122	0.144	2.12	0.010	0.044	88,824	0.045	0.408	2.41	0.107	0.539	424	22.6	0.619	209
114	1962	0.602	10.5	0.105	0.323	75,638	0.384	1.28	7.38	1.47	2.0	8520	328	9.94	190
115	1983	0.667	11.4	0.090	0.364	40,678	0.232	0.959	7.61	1.19	2.12	6664	327	5.01	125
116	3938	3.40	40.7	0.195	2.95	35,985	0.394	1.62	39.9	4.13	6.92	14,301	762	18.1	534
118	125	0.203	2.71	0.011	0.045	82,359	0.018	0.323	1.73	0.168	0.496	361.	42.2	1.11	274
119	2779	1.26	15.5	0.175	1.18	55,298	0.366	2.23	25.6	2.58	4.03	12,326	317	14.8	213
120	19.5	<0.100	13.1	<0.005	<0.030	79,182	0.067	0.319	11.6	<0.030	0.441	84.2	8.28	0.047	634
121	1851	0.804	31.8	0.105	0.884	72,333	0.147	1.15	6.50	1.69	2.10	4454	323	3.89	712
122	923	2.0	7.47	0.035	0.169	66,825	0.090	0.600	6.28	0.815	2.23	3845	767	1.09	396
123	105	0.205	1.57	0.011	0.044	69,173	0.020	0.309	2.70	0.064	0.462	459	63.5	0.100	6630
124	2396	2.13	21.0	0.138	0.715	54,126	0.505	1.37	8.49	1.25	3.58	8733	701	4.70	329
125	11.3	<0.100	0.545	<0.005	0.154	113,734	0.072	0.264	12.0	<0.030	0.298	77.5	4.67	0.068	10.3
126	1505	0.660	23.3	0.078	0.505	71,445	0.058	1.02	6.31	1.05	3.67	4241	461	3.23	379
127	11,202	7.18	76.1	0.503	2.46	15,950	0.323	5.84	35.8	6.55	7.68	28,640	1167	41.8	500
128	7388	3.74	63.5	0.370	1.71	28,058	0.213	3.69	17.8	5.56	6.65	20,436	1338	29.5	504
129	85.9	<0.100	0.917	<0.005	<0.030	94,922	0.047	0.319	2.52	0.069	0.460	257	14.6	0.300	19.4
130	4733	2.05	138	0.302	1.56	13,320	0.105	2.62	14.8	3.46	5.98	17,600	1502	15.2	1069
131	12.0	8.35	40.5	12.5	5.40	4.12	0.198	54.2	1.86	72.8	68.2	0.089	0.685	183	4.44
132	3.70	17.7	9.68	25.6	0.779	2.45	0.495	32.7	1.03	191	32.6	0.047	0.604	123	1.24
133	12.5	4.52	22.1	6.33	3.04	4.14	0.272	57.5	1.36	125	80.3	0.115	1.03	100	3.41
134	5.66	5.55	14.5	9.71	1.40	2.16	0.318	44.2	1.19	84.8	49.6	0.061	0.501	114	1.53
135	47.6	7.07	26.5	16.2	13.0	24.9	0.503	148	1.79	52.0	386	0.700	2.23	147	9.66
136	115	2.80	132	6.10	7.85	13.0	0.186	108	1.50	26.8	342	0.622	0.912	77.3	9.14
138	7.91	3.40	82.1	7.44	1.05	1.40	0.081	22.2	0.870	107	36.8	0.075	1.06	81.5	1.07
139	560	7.67	116	21.7	31.9	43.7	0.782	98.5	2.45	30.7	1068	1.62	4.29	212	24.5
140	11.0	3.98	16.0	6.85	0.730	1.64	0.250	20.4	0.523	11.3	38.3	0.079	0.292	69.6	0.892
141	73.3	5.07	11.7	6.83	1.43	0.898	0.150	18.7	1.19	47.0	40.2	0.131	0.600	113	1.27
142	477	8.24	36.0	18.0	20.2	22.9	0.656	80.7	1.63	38.7	496	1.18	2.25	98.1	14.0
143	0.767	5.0	29.6	7.35	0.251	0.176	0.359	2.76	1.35	116	5.41	0.009	0.975	137	0.711
144A	70.6	3.58	31.0	6.14	5.50	11.6	0.098	76.5	0.830	85.5	287	0.264	0.900	68.4	4.10
144B	16.1	5.08	15.2	7.20	0.827	0.650	0.039	15.0	1.22	93.4	29.0	0.038	0.870	104	0.739
145	126	5.45	17.3	7.50	6.76	7.66	0.202	106	0.772	18.1	214	0.308	0.920	76.7	5.08

Table A2. *Cont.*

Sample	Mn mg/kg	Mo mg/kg	Na mg/kg	Ni mg/kg	Pb mg/kg	Rb mg/kg	Sb mg/kg	Si mg/kg	Sn mg/kg	Sr mg/kg	Ti mg/kg	Tl mg/kg	U mg/kg	V mg/kg	Zn mg/kg
100	12.0	8.35	40.5	12.5	5.40	4.12	0.198	54.2	1.86	72.8	68.2	0.089	0.685	183	4.44
101	3.70	17.7	9.68	25.6	0.779	2.45	0.495	32.7	1.03	191	32.6	0.047	0.604	123	1.24
102	12.5	4.52	22.1	6.33	3.04	4.14	0.272	57.5	1.36	125	80.3	0.115	1.03	100	3.41
103	5.66	5.55	14.5	9.71	1.40	2.16	0.318	44.2	1.19	84.8	49.6	0.061	0.501	114	1.53
104	47.6	7.07	26.5	16.2	13.0	24.9	0.503	148	1.79	52.0	386	0.700	2.23	147	9.66
105	115	2.80	132	6.10	7.85	13.0	0.186	108	1.50	26.8	342	0.622	0.912	77.3	9.14
106	7.91	3.40	82.1	7.44	1.05	1.40	0.081	22.2	0.870	107	36.8	0.075	1.06	81.5	1.07
107	560	7.67	116	21.7	31.9	43.7	0.782	98.5	2.45	30.7	1068	1.62	4.29	212	24.5
108	11.0	3.98	16.0	6.85	0.730	1.64	0.250	20.4	0.523	11.3	38.3	0.079	0.292	69.6	0.892
109	73.3	5.07	11.7	6.83	1.43	0.898	0.150	18.7	1.19	47.0	40.2	0.131	0.600	113	1.27
110	477	8.24	36.0	18.0	20.2	22.9	0.656	80.7	1.63	38.7	496	1.18	2.25	98.1	14.0
111	0.767	5.0	29.6	7.35	0.251	0.176	0.359	2.76	1.35	116	5.41	0.009	0.975	137	0.711
112	70.6	3.58	31.0	6.14	5.50	11.6	0.098	76.5	0.830	85.5	287	0.264	0.900	68.4	4.10
113	16.1	5.08	15.2	7.20	0.827	0.650	0.039	15.0	1.22	93.4	29.0	0.038	0.870	104	0.739
114	126	5.45	17.3	7.50	6.76	7.66	0.202	106	0.772	18.1	214	0.308	0.920	76.7	5.08
115	108	4.62	19.9	8.03	6.37	7.23	0.180	113	0.939	11.1	351	0.313	0.915	89.6	4.55
116	111	126	32.8	204	75.0	35.8	0.474	201	2.76	68.7	530	0.603	2.19	162	18.6
118	2.78	3.61	11.7	5.20	0.645	1.08	1.03	20.6	1.39	131	25.8	0.053	0.833	82.3	0.772
119	251	70.7	16.7	107	18.0	14.8	0.531	157	1.87	32.5	525	0.414	2.39	138	11.2
120	0.982	37.1	11.5	51.0	0.203	0.180	0.383	2.90	0.847	4342	6.65	0.010	3.52	75.2	0.444
121	52.9	4.72	20.1	8.34	8.0	11.0	0.475	100	0.939	1127	204	0.425	1.18	78.6	3.53
122	9.33	16.4	17.0	22.0	2.78	10.6	0.191	135	0.888	103	162	0.041	1.31	108	1.64
123	6.35	7.93	13.2	9.14	0.265	0.838	0.205	13.9	1.05	65.4	10.7	0.022	1.13	111	0.755
124	85.5	9.89	20.7	16.3	10.1	16.7	0.383	127	1.66	38.5	461	0.247	2.0	111	7.58
125	0.234	54.3	4.32	107	0.243	0.076	0.226	1.43	0.689	10.2	2.98	0.045	0.170	92.8	0.535
126	43.6	3.30	26.1	7.46	5.61	9.10	0.201	119	1.03	76.5	204	0.260	0.940	86.0	3.57
127	215	9.47	44.6	22.9	29.7	38.4	0.811	104	2.40	44.5	754	1.91	3.26	124	25.0
128	312	5.46	84.7	17.0	24.9	33.8	0.507	112	2.28	50.5	658	1.27	3.09	118	18.4
129	2.28	6.46	7.22	13.6	0.433	0.448	0.035	8.52	0.812	8.44	18.6	0.028	0.239	161	0.851
130	145	3.55	204	9.55	17.6	37.7	0.380	122	1.79	45.4	486	0.602	1.34	107	12.7
131	8.49	461	18.6	658	1.10	2.23	0.108	48.9	0.921	28.9	65.0	0.095	0.365	94.5	1.77
132	1.62	46.6	12.6	63.8	0.600	0.903	0.284	14.5	1.0	80.6	16.2	0.015	1.43	122	0.848
133	168	6.07	70.3	10.9	23.7	31.5	0.360	119	2.14	73.8	613	0.420	2.02	124	12.3

Table A2. *Cont.*

Sample	Mn mg/kg	Mo mg/kg	Na mg/kg	Ni mg/kg	Pb mg/kg	Rb mg/kg	Sb mg/kg	Si mg/kg	Sn mg/kg	Sr mg/kg	Ti mg/kg	Tl mg/kg	U mg/kg	V mg/kg	Zn mg/kg
134	136	2.85	38.6	7.25	18.4	31.8	0.263	71.3	1.60	59.2	435	0.721	2.19	76.5	14.1
135	104	9.92	22.3	21.7	11.3	24.7	0.419	112	1.38	78.8	398	0.931	2.62	115	11.2
136	30.3	7.29	15.3	12.8	4.42	8.16	0.460	126	1.29	76.3	205	0.261	1.11	149	4.36
138	0.761	8.06	34.0	10.7	0.462	0.401	0.176	7.41	1.08	14.3	11.0	0.021	0.113	163	1.13
139	2.23	4.81	20.3	7.34	0.621	0.838	0.039	14.2	0.786	14.7	25.8	0.023	0.126	140	0.734
140	6.55	188	13.4	292	1.08	0.576	0.614	18.2	1.68	83.0	33.9	0.021	0.855	173	1.40
141	2.42	2.80	6.13	4.94	0.781	0.869	0.157	20.5	0.413	58.6	33.8	0.021	0.624	67.0	1.10
142	3.25	97.4	10.1	148	0.602	0.632	0.108	13.0	1.39	43.1	21.5	0.020	0.307	165	0.966
143	0.254	9.61	40.5	13.0	0.236	0.091	0.100	1.34	1.42	27.9	3.86	0.043	0.144	194	0.777
144A	0.385	5.84	10.5	9.43	0.222	0.113	0.084	1.98	0.833	22.5	2.17	0.040	0.056	122	0.660
144B	1.61	400	13.4	596	0.178	0.153	0.336	4.33	0.850	146	7.10	<0.003	1.43	157	0.530
145	1.08	7.67	176	10.9	0.324	0.230	0.313	6.45	1.73	113	9.88	0.005	2.53	168	1.17

Table A3. Results of ICP-MS and ion chromatography analysis of 30 chemical elements in three water samples.

Sample	Al µg/L	As µg/L	B µg/L	Ba µg/L	Be µg/L	Ca mg/L	Cd µg/L	Co µg/L	Cr µg/L	Cs µg/L	Cu µg/L	Fe µg/L	K mg/L	Li µg/L	Mg mg/L
W3	30.3	0.441	2.85	5.45	<0.005	37.1	0.020	0.097	0.260	<0.030	1.72	38.4	0.900	0.226	<0.500
W1	19.7	0.380	2.49	3.93	<0.005	34.8	<0.010	0.085	0.127	<0.030	2.33	13.7	0.200	0.227	<0.500
W2	64.1	0.355	2.85	3.70	<0.005	35.1	<0.010	0.090	0.162	<0.030	1.06	14.3	0.250	0.157	<0.500
MAC *	200	10	1500	700	n.a.	n.a.	5	n.a.	25	n.a.	2000	200	12	n.a.	n.a.

Sample	Mn µg/L	Mo µg/L	Na mg/L	Ni µg/L	Pb µg/L	Rb µg/L	Sb µg/L	Si mg/L	Sn µg/L	Sr µg/L	Ti µg/L	Tl µg/L	U µg/L	V µg/L	Zn µg/L
W3	1.22	0.088	0.860	0.557	0.411	0.475	0.207	1.30	0.060	29.0	0.732	0.004	0.212	0.443	1.58
W1	0.509	0.043	0.620	2.90	0.190	0.216	0.036	1.16	<0.020	30.1	0.579	<0.003	0.153	0.316	1.38
W2	0.607	0.065	0.610	0.649	<0.010	0.237	0.081	1.04	<0.020	27.8	0.534	<0.003	0.141	0.283	1.28
MAC *	50	n.a.	200	20	5	n.a.	10	n.a.	n.a.	n.a.	n.a.	n.a.	30	5	3000

Notes: * Ordinance on compliance parameters, methods of analysis, monitoring, and water safety plans for human consumption and method of keeping a register of legal entities performing the activity of public water supply (OG 64/2023). n.a.—Not analysed.

Table A4. Results of physico-chemical parameters, nutrients, ions, TN, TP, COD, and TOC in three water samples.

	W3	W1	W2	MAC *
pH	7.7	7.8	7.9	6.5–9.5
Conductivity (µScm⁻¹)	182	167	170	2500
TDS	122	112	114	n.a.

Table A4. *Cont.*

	W3	W1	W2	MAC *
Alkalinity (mgCaCO$_3$L^{-1})	90	84	87	n.a.
Total Hardness (mgCaCO$_3$L^{-1})	94.4	88.5	89	n.a.
HCO$_3^-$ (mgL^{-1})	110	102	106	n.a.
Turbidity (NTU)	16.2	0.75	0.87	4
Ammonium (mgNL^{-1})	0.017	<0.008	<0.008	0.5
Nitrates (mgNL^{-1})	0.81	0.74	0.77	50
Nitrites (mgNL^{-1})	<0.002	<0.002	<0.002	0.5
Orthophosphates (mgPL^{-1})	0.007	<0.005	0.005	0.3
Sulphates (mgL^{-1})	1.7	2.1	1.7	250
Chlorides (mgL^{-1})	1.82	1.0	1.07	250
Fluorides (mgL^{-1})	<0.025	<0.025	<0.025	1.5
TP (mgPL^{-1})	0.008	<0.003	0.016	n.a.
TN (mgNL^{-1})	1.08	0.83	0.95	n.a.
COD (mgL^{-1})	1.3	<0.7	<0.7	5
TOC (mgL^{-1})	2.21	0.45	0.58	n.a.

Notes: * Ordinance on compliance parameters, methods of analysis, monitoring, and water safety plans for human consumption and method of keeping a register of legal entities performing the activity of public water supply (OG 64/2023). n.a.—Not analysed.

Table A5. Magnetic susceptibility measured in cave samples from Velebit Mt.

Sample	100	101	102	103	104	105	106	107	108	109	110
MS (10^{-3} SI units)	0.008	0.000	0.014	0.000	0.047	0.043	0.002	0.168	0.002	0.001	0.064
Sample	111	112	113	114	115	116	118	119	120	121	122
MS (10^{-3} SI units)	0.000	0.094	0.000	0.026	0.009	0.070	0.000	0.038	0.000	0.033	0.005
Sample	124	125	126	127	128	129	130	131	132	133	134
MS (10^{-3} SI units)	0.015	0.001	0.099	0.024	0.069	0.002	0.152	0.003	0.002	0.089	0.060
Sample	135	136	138	139	140	141	142	143	144A	144B	145
MS (10^{-3} SI units)	0.042	0.008	0.002	0.005	0.001	0.000	0.003	0.000	0.002*	0.001*	0.000

* $p < 0.05$.

Table A6. Members of obtained clusters and distances from respective cluster centers.

Cluster Number 1		Cluster Number 2		Cluster Number 3	
	Distance		Distance		Distance
100	2296.907	101	986.315	107	3840.709
102	1160.563	103	1949.649	110	707.108
104	3505.504	105	1746.685	115	3650.59
112	780.491	106	5148.341	116	2335.307

Table A6. *Cont.*

Cluster Number 1		Cluster Number 2		Cluster Number 3	
	Distance		Distance		Distance
114	1327.349	108	2782.85	127	2383.742
118	2442.552	109	1859.763	128	995.872
119	2682.862	111	1447.447	130	1696.761
120	2068.802	113	1608.54	133	630.79
121	615.082	125	2667.503	134	857.839
122	428.126	129	568.616		
123	1283.476	131	1669.34		
124	2634.997	132	1892.675		
126	454.429	138	241.428		
135	3506.321	139	113.224		
136	979.731	140	851.933		
141	2363.343	142	923.613		
		143	1501.29		
		144A	1315.248		
		144B	1271.849		
		145	274.117		

Table A7. Mean values of 10 elements and two other parameters for 3 obtained clusters. Elements' contents are given in mg/kg, elevation in m.

	Cluster—No. 1	Cluster—No. 2	Cluster—No. 3
Depth	664.25	440.25	323.89
Al	1402.22	352.46	6420.78
B	1.04	0.86	4.40
Ba	17.68	5.55	79.56
Be	0.08	0.02	0.32
Bi	0.48	0.10	1.72
Ca	68,916.31	98,196.25	23,043.11
Cd	0.13	0.13	0.26
Co	0.91	0.46	3.06
Cr	7.50	23.33	30.18
Cs	1.47	5.56	4.00
Cu	2.24	0.75	5.82
Fe	4795.51	644.85	17,686.45
K	353.35	101.23	1105.11
Li	4.90	1.24	20.72
Mg	725.63	153.69	608.00
Mn	53.62	13.11	248.00
Mo	12.66	66.92	19.33
Na	19.88	33.59	71.88

Table A7. *Cont.*

	Cluster—No. 1	**Cluster—No. 2**	**Cluster—No. 3**
Ni	19.66	100.34	35.48
Pb	5.99	1.02	27.53
Rb	9.40	1.45	31.43
Sb	0.36	0.22	0.49
Si	86.01	20.21	113.50
Sn	1.21	1.10	2.00
Sr	405.19	63.50	46.96
Ti	204.47	39.59	599.00
Tl	0.26	0.07	0.96
U	1.46	0.68	2.39
V	106.01	128.59	123.47
Zn	4.55	1.40	16.02

Table A8. Factor loadings (varimax normalized; marked loadings are >0.7).

	Factor—1	**Factor—2**	**Factor—3**
Depth	−0.124302	−0.023993	−0.819019
Al	0.954821	0.040576	0.065068
Be	0.964641	0.013376	0.052559
Ca	−0.910654	−0.035486	0.071048
Cd	0.367832	0.870409	0.002824
Co	0.943561	0.088319	0.060373
Cr	0.097057	0.956666	0.030635
Cu	0.965842	0.043518	0.106860
Fe	0.987710	0.045008	0.063385
Li	0.928842	0.059540	0.121091
Mn	0.860786	0.107496	0.059534
Ni	−0.183442	0.940852	0.034932
Pb	0.792268	0.117471	0.138042
Si	0.722576	0.023701	0.062805
Sr	−0.060724	−0.024627	−0.804648
Zn	0.979650	0.057248	0.111071
Expl.Var	9.380962	2.606750	1.405087
Prp.Totl	0.586310	0.162922	0.087818

Table A9. Factor scores for analyzed samples.

	Factor—1	**Factor—2**	**Factor—3**
100	−0.44969	−0.468335	0.91344
101	−0.66168	−0.423453	0.83505

Table A9. *Cont.*

	Factor—1	Factor—2	Factor—3
102	−0.44930	−0.507157	0.74082
103	−0.61171	−0.481194	0.81870
104	0.65183	−0.469277	0.74884
105	0.34543	−0.280647	0.72149
106	−0.77655	−0.455562	0.83723
107	2.91683	0.220452	0.07686
108	−0.76396	−0.477140	0.54742
109	−0.59976	−0.389911	0.39858
110	1.57251	1.230746	0.06671
111	−0.80161	−0.501358	0.12572
112	−0.03876	−0.442072	−0.02598
113	−0.68940	−0.468341	0.36007
114	0.18179	0.138592	0.29450
115	0.16931	−0.151257	0.20318
116	1.48445	0.983193	0.95783
118	−0.70573	−0.550535	0.84204
119	0.88586	0.531137	0.26291
120	−0.34931	−0.095727	−4.94046
121	0.13086	−0.249879	−2.03191
122	−0.13940	−0.339670	−1.09632
123	−0.56206	−0.484421	−1.03985
124	0.47950	0.399545	−1.17644
125	−0.87972	−0.012148	0.13909
126	−0.01168	−0.483615	0.24995
127	2.75371	0.126628	0.10225
128	1.96719	−0.195167	0.15930
129	−0.76242	−0.443131	0.47835
130	1.28806	−0.439484	0.58186
131	−0.82480	4.817560	−0.06662
132	−0.72776	0.154602	0.02479
133	1.22900	−0.462031	−0.21315
134	1.10399	−0.353444	−0.18035
135	0.67268	−0.338948	−0.41738
136	−0.08725	−0.449788	−0.31604
138	−0.71929	−0.485320	−0.28463
139	−0.70896	−0.517329	−0.27965
140	−0.74195	1.245226	−0.42709
141	−0.59604	−0.507463	−0.55998
142	−0.72349	0.332592	−0.55415
143	−0.86040	−0.486455	0.96571

Table A9. *Cont.*

	Factor—1	Factor—2	Factor—3
144A	−0.85409	−0.514546	0.99775
144B	−1.02319	3.184189	0.74276
145	−0.71303	−0.439658	−0.58319

Table A10. Correlations between MS and determined chemical elements. Correlations are significant at $p < 0.05000$. N = 45—marked in red.

	Al	B	Ba	Be	Bi	Ca	Cd	Co	Cr	Cs	Cu	Fe	K	Li	Mg
MS	0.73	0.59	0.87	0.75	0.71	−0.75	0.19	0.69	0	−0.01	0.8	0.74	0.84	0.57	0.09
	Mn	Mo	Na	Ni	Pb	Rb	Sb	Si	Sn	Sr	Ti	Tl	U	V	Zn
MS	0.7	−0.15	0.56	−0.14	0.6	0.81	0.31	0.59	0.53	−0.1	0.78	0.64	0.51	0.04	0.72

References

1. Bognar, A.; Faivre, S.; Buzjak, N.; Pahernik, M.; Bočić, N. Recent Landform Evolution in the Dinaric and Pannonian Regions of Croatia. In *Recent Landform Evolution: The Carpatho–Balkan–Dinaric Region*; Lóczy, D., Stankoviansky, M., Kotarba, A., Eds.; Springer: Cham, Switzerland, 2012; pp. 313–344.
2. White, W.B. *Cave Geology*; Cambridge University Press: Cambridge, UK, 2007.
3. Sasowsky, I.D.; Mylroie, J. *Studies of Cave Sediments: Physical and Chemical Records of Paleoclimate*; Springer: Dordrecht, The Netherlands, 2004.
4. Paar, D.; Frančišković-Bilinski, S.; Buzjak, N.; Maldini, K.; Milović, S.; Pichler, S. Geochemical and Mineralogical Characterization of Speleothems from the Karst of Croatia as Potential Sources of Data for Environmental Research. *J. Geochem. Explor.* **2016**, *167*, 20–37. [CrossRef]
5. Surić, M. Speleothem-Based Quaternary Research in Croatian Karst—A Review. *Quat. Int.* **2018**, *490*, 113–122.
6. Höpker, R.; Müller, T.; Schmidt, F.; Becker, J. Recent Developments in Cave Sediment Studies. *J. Karst Res.* **2024**, *58*, 233–245.
7. Çil, E.; Kaya, Ö.; Yılmaz, H.; Demir, A. Speleothem Geochemistry and Paleoenvironmental Interpretations. *Earth Sci. J.* **2023**, *49*, 120–135.
8. Muri, G.; Kralj, P.; Krajcar Bronić, I.; Horvatinčić, N. Karst Aquifers and Their Vulnerability to Contamination. *Hydrogeol. J.* **2013**, *21*, 765–779.
9. Chen, J.; Wang, S.; Liu, Y.; Zhang, Q.; Zhao, H. Groundwater Extraction from Karst Aquifers: A Global Perspective. *Water Resour. Res.* **2017**, *53*, 890–905.
10. Kuhta, M.; Brkić, M. Hydrogeochemical Dynamics of Karst Systems. *Environ. Geol.* **2008**, *56*, 567–580.
11. Paar, D.; Mance, D.; Stroj, A.; Pavić, M. Northern Velebit (Croatia) Karst Hydrological System: Results of a Preliminary ^{2}H and ^{18}O Stable Isotope Study. *Geol. Croat.* **2019**, *72*, 205–213.
12. Addesso, R.; De Waele, J.; Cafaro, S.; Baldantoni, D. Geochemical Characterization of Clastic Sediments Sheds Light on Energy Sources and on Alleged Anthropogenic Impacts in Cave Ecosystems. *Int. J. Earth Sci.* **2022**, *111*, 919–927.
13. Rozkowski, J.; Rozkowski, K.; Rahmonov, O. Heavy Metals in the Unsaturated and Saturated Zone of the Upper Jurassic Carbonate Massif in the Vicinity of Krakow. *J. Elementol.* **2015**, *20*, 395–406.
14. Pons-Branchu, E.; Takahashi, C.; Frisia, S.; Borsato, A. Urban Speleothems as Records of Heavy Metal Pollution. *Sci. Total Environ.* **2015**, *512*, 435–448.
15. Allan, M.; Fagel, N.; Van Rampelbergh, M.; Baldini, J.; Riotte, J.; Cheng, H.; Edwards, R.L.; Gillikin, D.; Quinif, Y.; Verheyden, S. Lead Concentrations and Isotope Ratios in Speleothems as Proxies for Atmospheric Metal Pollution Since the Industrial Revolution. *Chem. Geol.* **2015**, *401*, 140–150.
16. Xu, H.; Li, Y.; Wang, X.; Zhang, L. Heavy Metal Contamination in Cave Water Systems. *Hydrogeol. Contam. Transp.* **2020**, *12*, 123–135.
17. Zeng, J.; Han, G.L.; Yang, K.H. Assessment and Sources of Heavy Metals in Suspended Particulate Matter in a Tropical Catchment, Northeast Thailand. *J. Clean. Prod.* **2020**, *265*, 121898. [CrossRef]
18. Zupan Hajna, N. Speleothem Records and Karst Hydrology. *J. Karst Hydrogeol.* **2011**, *28*, 403–415.
19. Surić, D.; Barešić, J.; Lončar, T.; Peh, Z. Evolution of Speleothem Deposition in Croatian Caves: Implications for Paleoenvironmental Changes. *J. Karst Geochem.* **2005**, *21*, 105–120.

20. Surić, D.; Perica, D.; Tibljaš, D. Multi-Year Geochemical Analysis of Speleothems: A New Perspective on Karst Hydrology. *Geochim. Cosmochim. Acta* **2009**, *73*, 245–260.

21. Bonacci, O. *Karst Hydrology: With Special Reference to Dinaric Karst*; Springer: Berlin/Heidelberg, Germany, 1987.

22. Boldrin, A.; Juračić, M.; Mengazzo Vitturi, L.; Rabitti, S.; Rampazzo, G. Sedimentation of River-Borne Material in a Shallow Shelf Sea: Adiga River, Adriatic Sea. *Mar. Geol.* **1992**, *103*, 473–485. [CrossRef]

23. Gupta, S.K. *Modern Hydrology and Sustainable Water Development*; Wiley & Sons—Blackwell Publishing: Hoboken, NJ, USA, 2011.

24. Boyd, C.E. Carbon Dioxide, pH and Alkalinity. In *Water Quality*; Springer: Cham, Switzerland, 2020.

25. StatSoft, Inc. *STATISTICA (Data Analysis Software System), Version 6*; StatSoft, Inc.: Tulsa, OK, USA, 2001. Available online: www.statsoft.com (accessed on 20 February 2025).

26. Tukey, J.W. *Exploratory Data Analysis*; Addison-Wesley: Reading, PA, USA, 1977.

27. Reimann, C.; Filzmoser, P.; Garrett, R.G. Background and Threshold: Critical Comparison of Methods of Determination. *Sci. Total Environ.* **2005**, *346*, 1–16. [CrossRef]

28. Kaufman, L.; Rousseeuw, P. *Finding Groups in Data*; John Wiley & Sons: New York, NY, USA, 1990.

29. Halamić, J.; Peh, Z.; Bukovec, D.; Miko, S.; Galović, L. A Factor Model of the Relationship Between Stream Sediment Geochemistry and Adjacent Drainage Basin Lithology, Medvednica Mt., Croatia. *Geol. Croat.* **2001**, *54*, 37–51. [CrossRef]

30. Davis, J.C. *Statistics and Data Analysis in Geology*, 3rd ed.; John Wiley & Sons: Hoboken, NJ, USA, 2002.

31. Frančišković-Bilinski, S.; Scholger, R.; Bilinski, H.; Tibljaš, D. Magnetic, Geochemical and Mineralogical Properties of Sediments from Karst and Flysch Rivers of Croatia and Slovenia. *Environ. Earth Sci.* **2014**, *72*, 3939–3953.

32. Chen, B.; Wang, F.; Shi, J.; Chen, F.; Shi, H. Origin and Sources of Minerals and Their Impact on the Hydrocarbon Reservoir Quality of the PaleogeneLulehe Formation in the Eboliang Area, Northern Qaidam Basin, China. *Minerals* **2019**, *9*, 436. [CrossRef]

33. Stroj, A.; Velić, I. Geological Profile of the Lukina Jama–Trojama Cave System in Northern Velebit. In Proceedings of the 5th Croatian Geological Congress—Book of Abstracts, Osijek, Croatia, 23–25 September 2015; Croatian Geological Institute: Zagreb, Croatia, 2015; pp. 240–241.

34. Frančišković-Bilinski, S. Detection of Coal Combustion Products in Stream Sediments by Chemical Analysis and Magnetic-Susceptibility Measurements. *Mineral. Mag.* **2008**, *72*, 43–48.

35. Durn, G.; Aljinović, D.; Crnjaković, M.; Lugović, B. Heavy and light mineral fractions indicate polygenesis of extensive terra rossa soils in Istria, Croatia. In *Heavy Minerals in Use*; Elsevier: Amsterdam, The Netherlands, 2007; pp. 701–737.

36. Pons-Branchu, E.; Ayrault, S.; Roy-Barman, M.; Bordier, L.; Borst, W.; Branchu, P.; Douville, E.; Dumont, E. Three Centuries of Heavy Metal Pollution in Paris (France) Recorded by Urban Speleothems. *Sci. Total Environ.* **2015**, *518*, 86–96.

37. Matić, N.; Miklavčić, I.; Maldini, K.; Tomas, D.; Cuculić, V.; Cardellini, C.; Frančišković-Bilinski, S. Geochemical and Isotopic Characteristics of Karstic Springs in Coastal Mountains (Southern Croatia). *J. Geochem. Explor.* **2013**, *132*, 90–110.